iScience

CellPress
OPEN ACCESS

Article

Immune perturbation network identifies an EMT subtype with chromosomal instability and tumor immune-desert microenvironment

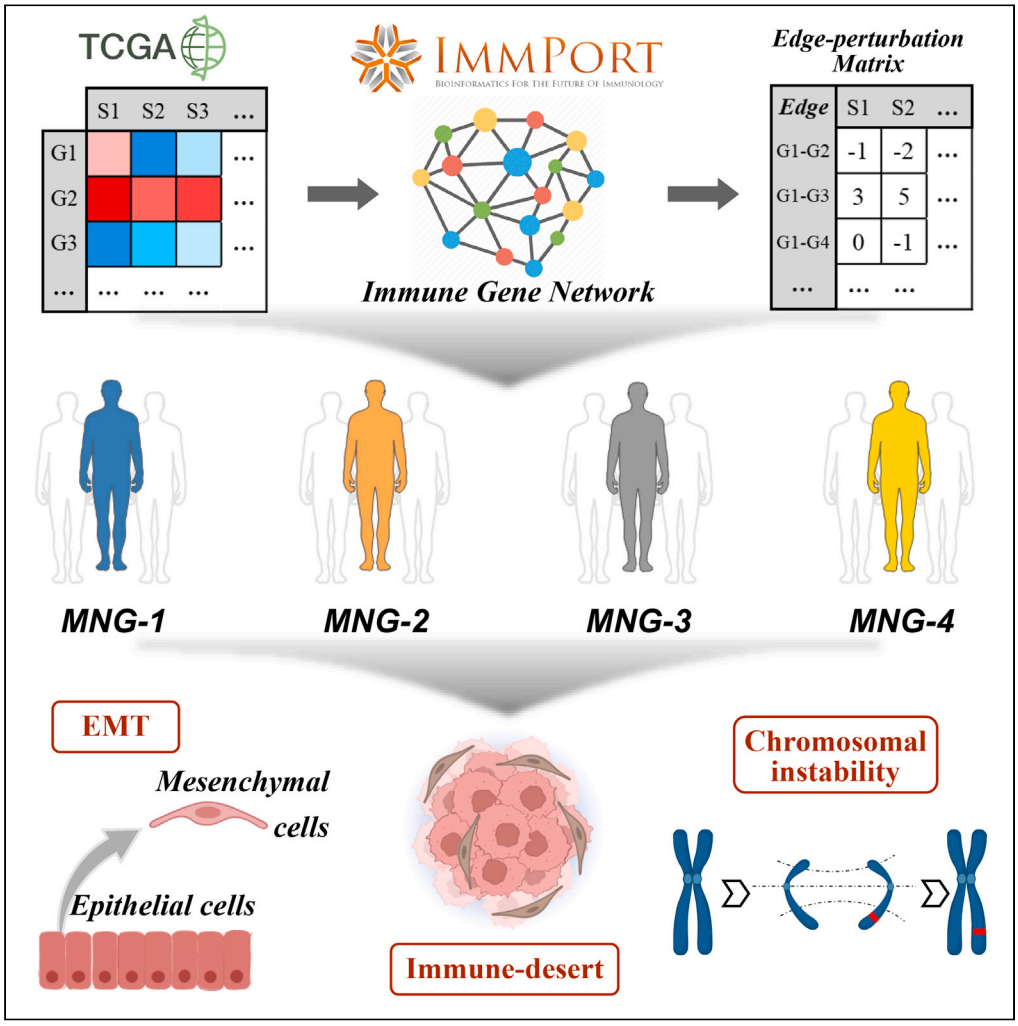

Hui Xu, Xinyu Fu, Ben Liu, ..., Kexin Chen, Zaoqu Liu, Xinwei Han

chenkexin@tmu.edu.cn (K.C.)
liuzaoqu@163.com (Z.L.)
fcchanxw@zzu.edu.cn (X.H.)

Highlights

Exploration of GC heterogeneity based on global immune gene background network

Dynamic changes and interactions in gene expression were considered in the study

A subtype with poor prognosis, EMT, CIN, and immune-desert was identified

Xu et al., iScience 26, 107871
October 20, 2023 © 2023
https://doi.org/10.1016/j.isci.2023.107871

iScience

CellPress
OPEN ACCESS

Article

Immune perturbation network identifies an EMT subtype with chromosomal instability and tumor immune-desert microenvironment

Hui Xu,[1,12] Xinyu Fu,[2,12] Ben Liu,[3,12] Siyuan Weng,[1,12] Chunguang Guo,[4] Libo Quan,[5] Long Liu,[6] Libo Wang,[6] Zhe Xing,[7] Quan Cheng,[8] Peng Luo,[9] Kexin Chen,[3,*] Zaoqu Liu,[10,11,*] and Xinwei Han[1,13,*]

SUMMARY

Most gastric cancer (GC) subtypes are identified through transcriptional profiling overlooking dynamic changes and interactions in gene expression. Based on the background network of global immune genes, we constructed sample-specific edge-perturbation matrices and identified four molecular network subtypes of GC (MNG). MNG-1 displayed the best prognosis and vigorous cell cycle activity. MNG-2 was enriched by immune-hot phenotype with the potential for immunotherapy response. MNG-3 and MNG-4 were identified with epithelial-mesenchymal transition (EMT) peculiarity and worse prognosis, termed EMT subtypes. MNG-3 was characterized by low mutational burden and stromal cells and considered a replica of previous subtypes associated with poor prognosis. Notably, MNG-4 was considered a previously undefined subtype with a dismal prognosis, characterized by chromosomal instability and immune-desert microenvironment. This subtype tended to metastasize and was resistant to respond to immunotherapy. Pharmacogenomics analysis showed three therapeutic agents (NVP-BEZ235, LY2606368, and rutin) were potential interventions for MNG-4.

INTRODUCTION

Gastric cancer (GC) is a highly prevalent and deadly cancer, ranking fifth in incidence and second in mortality.[1] Unfortunately, most patients are diagnosed at advanced stages due to its atypical early manifestations, resulting in a dismal prognosis.[2] Despite significant progress in treatment options such as surgery, chemotherapy, targeted therapy, and immunotherapy, the mortality rate remains alarmingly high.[3] Moreover, clinical management is a significant challenge as patients with the same pathologic stage can have vastly different prognoses with the same treatment method.[4] This issue arises from conventional clinicopathological staging that overlooks clinical heterogeneity and molecular biology, leading to overtreatment or undertreatment.[5]

With the continuous innovation of sequencing technology and bioinformatics, numerous molecular subtypes of GC have been identified and investigated, such as "Singapore-Duke" subtypes derived from the differences in gene expression patterns,[6] The Cancer Genome Atlas (TCGA) subtypes based on multi-omics,[7] Asian Cancer Research Group (ACRG) subtypes closely related to clinical outcomes,[8] as well as mesenchymal phenotype (MP) and epithelial phenotype (EP) proposed by Sang et al.[9] These significant efforts have expanded our understanding of basic GC biology and the heterogeneity inherent to this disease. Despite clear disclosure of driver mutations like TP53, kirsten rats arcomaviral oncogene homolog (KRAS), and HER-2 in multiple molecular subtypes, clinical efforts to target these alterations have yielded different results, hampered by complex co-alteration patterns in molecular profiles and genomic heterogeneity within patients.[10] Noteworthily, gene expression is a dynamic process subject to temporal and spatial disturbances, rendering molecular subtypes constructed solely based on gene expression profiles impractical in clinical practice.[11,12] To overcome this limitation, the gene network, which considers both

[1]Department of Interventional Radiology, The First Affiliated Hospital of Zhengzhou University, Zhengzhou, Henan 450052, China
[2]Genetic and Prenatal Diagnosis Center, The First Affiliated Hospital of Zhengzhou University, Zhengzhou, China
[3]Key Laboratory of Molecular Cancer Epidemiology of Tianjin, Department of Epidemiology and Biostatistics, National Clinical Research Center for Cancer, Tianjin Medical University Cancer Institute and Hospital, Tianjin 300060, China
[4]Department of Endovascular Surgery, The First Affiliated Hospital of Zhengzhou University, Zhengzhou, Henan 450052, China
[5]Department of Gastroenterology and Hepatology, First Affiliated Hospital of Zhengzhou University, Zhengzhou, Henan 450052, China
[6]Department of Hepatobiliary and Pancreatic Surgery, The First Affiliated Hospital of Zhengzhou University, Zhengzhou, Henan, China
[7]Department of Neurosurgery, The Fifth Affiliated Hospital of Zhengzhou University, Zhengzhou, China
[8]Department of Neurosurgery, Xiangya Hospital, Central South University, Changsha, China
[9]Department of Oncology, Zhujiang Hospital, Southern Medical University, Guangzhou, China
[10]State Key Laboratory of Proteomics, Beijing Proteome Research Center, National Center for Protein Sciences (Beijing), Beijing Institute of Lifeomics, Beijing 102206, China
[11]State Key Laboratory of Medical Molecular Biology, Institute of Basic Medical Sciences, Chinese Academy of Medical Sciences, Department of Pathophysiology, Peking Union Medical College, Beijing, 100730, China
[12]These authors contributed equally
[13]Lead contact
*Correspondence: chenkexin@tmu.edu.cn (K.C.), liuzaoqu@163.com (Z.L.), fcchanxw@zzu.edu.cn (X.H.)
https://doi.org/10.1016/j.isci.2023.107871

gene nodes and interactions, can provide stable gene expression states and result in molecular subtypes exhibiting strong robustness and repeatability.[13,14]

Like other solid tumors arising from epithelial cells, immune cells in the microenvironment surrounding GC cells play an unignored role in tumor progression and development. GC has emerged as a paradigm for inflammation-driven cancers due to the critical impact of immune infiltration creating and shaping the tumor immune microenvironment (TIME) that promotes GC progression.[15–17] Although clinical studies of immunotherapy for GC are in full swing, non-response and adverse reactions to this therapy are common in clinical practice.[18] However, several previously published major molecular subtypes lacking exploration of immunotherapy and limited availability of common immunotherapeutic markers lead to the challenge for individual precision of this therapy.[10] Therefore, developing immune gene network-driven GC molecular subtypes helps explore tumor heterogeneity further and provides potential immunotherapy implications.

In this study, we successfully constructed a stable gene network based on the interaction of the immune genes and identified four network-based molecular subtypes. Subsequently, we adequately assessed the robustness of the molecular subtypes in four public cohorts and an in-house cohort. Meanwhile, the underlying biological characteristics, genomic alterations, and immune abundance in different subtypes were explored, and the optimal treatments were formulated. Overall, gene network-based molecular subtypes have potent classification capabilities, promoting the stratified management and precise treatment of GC patients in clinical practice.

RESULTS

Construction of the immune gene interaction network subtypes

The study flowchart is shown in Figure S1. Based on the ImmPort Portal and search tool for recurring instances of neighbouring genes (STRING) database, 1,793 immune genes and 15,347 gene pairs were generated (Table S2). Subsequently, we screened each gene pair based on the established edge-perturbation pipeline. Our findings support the earlier hypothesis that immune genes are more perturbed in tumor samples than in normal samples ($p = 1.4e-5$, Figures 1A and 1B). Additionally, the constructed background network closely approximates the distribution of a scale-free biological network (Figure 1C). The edge-perturbation matrix was created based on 6,559 edge-perturbations from 348 GC samples. These gene pairs were used as features of unsupervised clustering for subsequent analysis.

With the optimal number of k selected according to the cumulative distribution function curve (Figure 1D), consensus clustering identified four subtypes sourced from the molecular network of GC (MNG) in the TCGA cohort. To further investigate the differences in survival prognosis among the four subtypes, we evaluated the four subtypes from overall survival (OS), disease-specific survival (DSS), relapse-free survival (RFS), and progression-free survival (PFS), respectively. As illustrated in Figures 1E–1H, survival curves showed that the prognosis of patients with the four subtypes showed significant and consistent differences (OS: $p = 4e-04$; DSS: $p = 0.0351$; RFS: $p = 0.0219$; PFS: $p = 8e-04$). From subtype MNG-1 to MNG-4, the prognosis was progressively depressed, especially MNG-4 with the poorest prognosis.

Validation of the subtypes and association with previous GC classifications

Differential expression analysis showed that the top 1,000 overexpressed genes in each subtype were candidate signature genes. Further multiple comparison testing identified 238 genes as subtype specific (Table S3), which the nearest template prediction (NTP) algorithm utilized to identify patient-belonging subtypes in four public datasets. SubMap subsequently validated the accuracy of the assignation of subtypes from the perspective of gene expression profile similarity (Figure S2A). In addition, the prognostic analysis of OS in GSE15459 ($p = 0.0106$) and GSE26253 ($p = 0.0473$) was also consistent with the discovery cohort (Figures 2A and 2B), but that in GSE84433 ($P = 4e-04$) and GSE84437 ($P = 3e-04$) was partially compatible (Figures S2B and S2C). Therefore, we included the Tianjin cohort for further validation. Similar to the previous results, characteristic genes were significantly highly expressed in the corresponding identified subtype (Figure 2C), and the expression profiles of the same subtype were significantly similar between the discovery and Tianjin cohorts (Figure S2D). MNG-4 showed the most dismal prognosis of both OS ($p = 0.0052$) and RFS ($p = 0.0014$), while MNG-1 performed the best prognosis (Figures 2D and 2E). In conclusion, the results proved the robustness of the MNG classifier and the accordance of the prognosis among subtypes.

Due to American Joint Committee on Cancer (AJCC)/Union for International Cancer Control (UICC) staging system being widely used as the primary reference in determining the clinical treatment for GC, we compared the composition and proportion of each stage between different subtypes. From MNG-1 to MNG-4, the proportion of Stage IV gradually increased, consistent with the gradual deterioration of the prognosis (Figures 2F and S2E). The Cox regression analysis also displayed that the MNG-1 subtype is a favorable factor for prognosis while MNG-4 is an unfavorable one, further confirming the prognostic value of MNG subtypes (Figures 2G and 2H). Furthermore, samples from TCGA datasets were assigned into previous subtypes based on the TCGA network study, ACRG study, gastrointestinal tract adenocarcinomas (GIACs) study, histologic Lauren subtype, and Sang et al.[7–9,19] We observed significant correlations between MNG classification and previous classifications, revealing a molecular convergence (Figure S2F). Chromosomal instability (CIN) samples accounted for the highest proportion of the MNG-4 subtype in both TCGA and GIACs studies, while genome stable (GS) tended to cluster in the MNG-3 subtype. Notably, MP, epithelial-mesenchymal transition (EMT), and Diffuse subtypes, which respond to poor prognosis, are mainly clustered in the MNG-3 subtype, implying that MNG-4 may be an undefined but different poor prognostic subtype compared with the previous subtypes.

Subtype-specific functional phenotypes of MNG subtypes

Gene set variation analysis (GSVA) is a gene set expression-based analysis method used to score the enrichment of a given gene set in a sample, performed to convert the gene expression matrix to the pathway score matrix in this study. We performed the differential analysis of

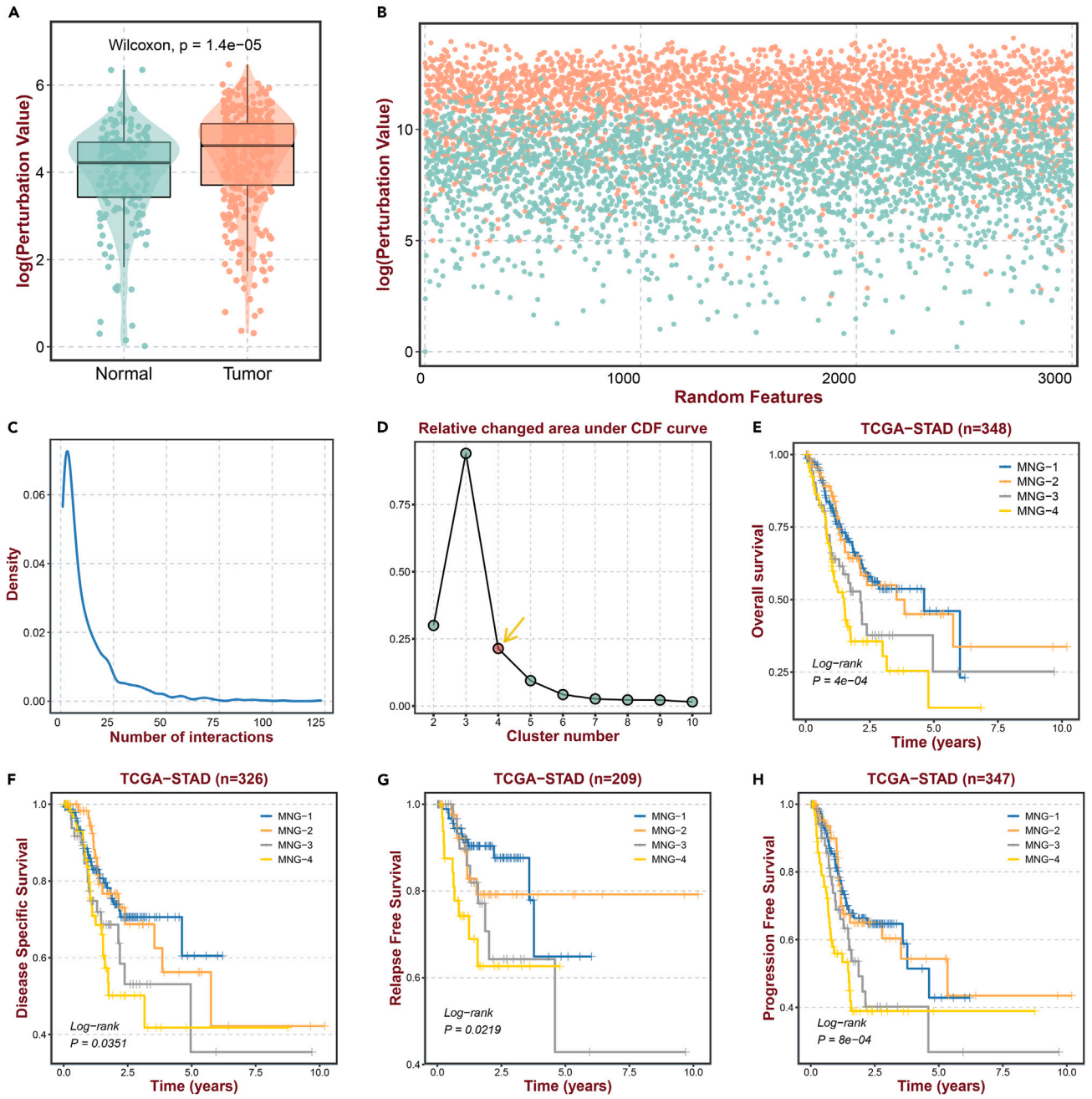

Figure 1. The identification of four gastric cancer (GC) molecular subtypes

(A) The differential comparison of perturbation value between the tumor and normal samples.

(B) The scatterplot for the log2-transformed mean of the interaction perturbations in the 3,000 randomly selected edges in normal (green points) and GC (red points) tissues.

(C) The constructed background network fitted the scale-free biological network distribution.

(D) The cumulative distribution function (CDF) curve helped to determine the optimal number of clusters for the Consensus Cluster. The red dot indicated by the arrow is the location of the optimal number of clusters.

(E–H) Kaplan-Meier survival analysis of MNG subtypes based on overall survival (OS), disease-specific survival (DSS), relapse-free survival (RFS), and progression-free survival (PFS) in the TCGA cohort.

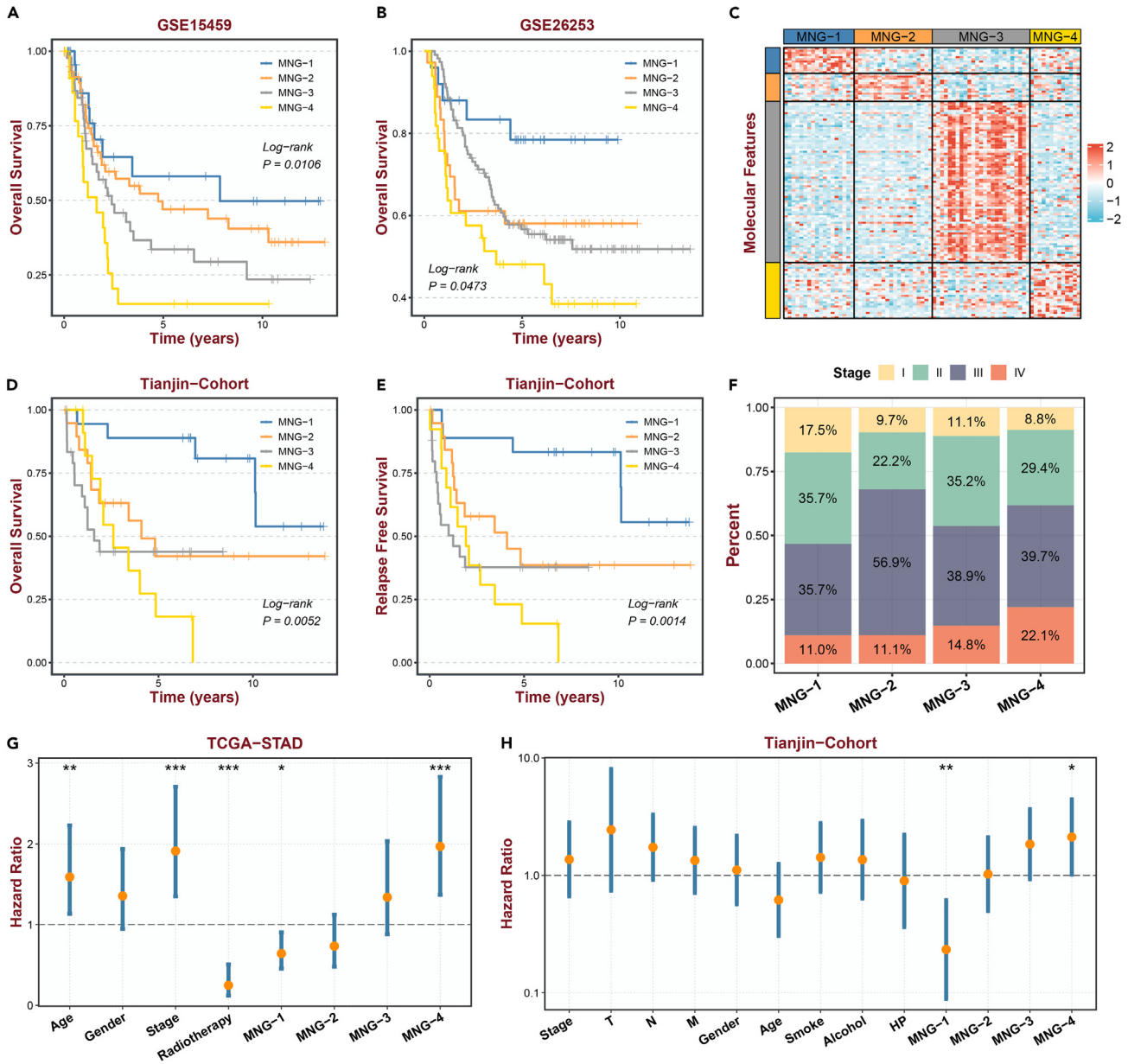

Figure 2. Validation of the subtypes in five independent cohorts and prognosis exploration

(A and B) Kaplan-Meier (KM) survival analysis of MNG subtypes based on overall survival (OS) in GSE15459 (A) and GSE26253 (B).

(C) The subtype-specific gene expression heatmap of the MNG subtypes in the Tianjin cohort.

(D and E) KM OS (D) curves and relapse-free survival (F) according to MNG subtypes in the Tianjin cohort.

(F) The proportion of AJCC Stage for each MNG subtype in the TCGA cohort.

(G and H) Univariate Cox regression analysis of MNG classification and other clinical traits in TCGA (G) and Tianjin (H) cohorts. *p < 0.05, **p < 0.01, and ***p < 0.001. See also Figure S2.

functional scores and selected pathways with significant differences to characterize each subtype, these pathways also being proved to be enriched via gene set enrichment analysis (GSEA) (Figure 3A). Pathways that tend to be enriched in the MNG-1 subtype are cell cycle-related and represented by E2F targets, DNA replication, and mitotic sister chromatid segregation (Figures 3A and S3A). Notably, protective pathways like the G2M checkpoint are also enriched in MNG-1 isoforms. The MNG-2 subtype was mainly enriched with immune pathways, such as antigen binding, T cell receptor complex, and immune response activation (Figures 3A and S3B). The MNG-4 and MNG-3 subtypes with poor prognoses were enriched with the tumor-promoting associated pathways, such as EMT and extracellular matrix (ECM) receptor interaction

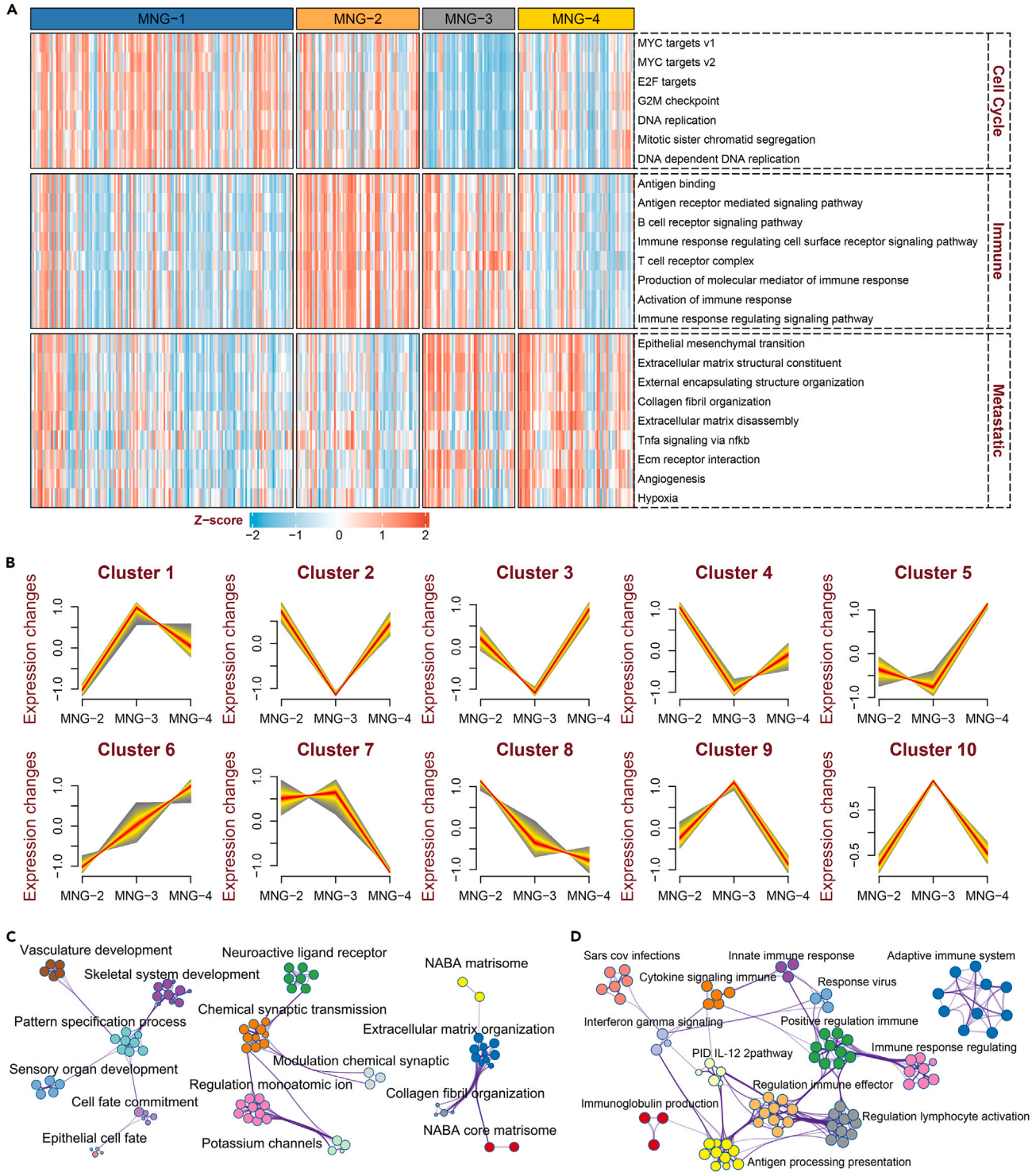

Figure 3. Biological function exploration for each subtype

(A) Heatmap of enriched functional pathway scores for each MNG subtype derived from gene set variation analysis.

(B) The *Mfuzz* algorithm identified ten gene clusters in MNG-2/3/4 subtypes.

(C and D) Metascape functional analysis of feature genes from Cluster 6 (C) and Cluster 8 (D). See also Figure S3.

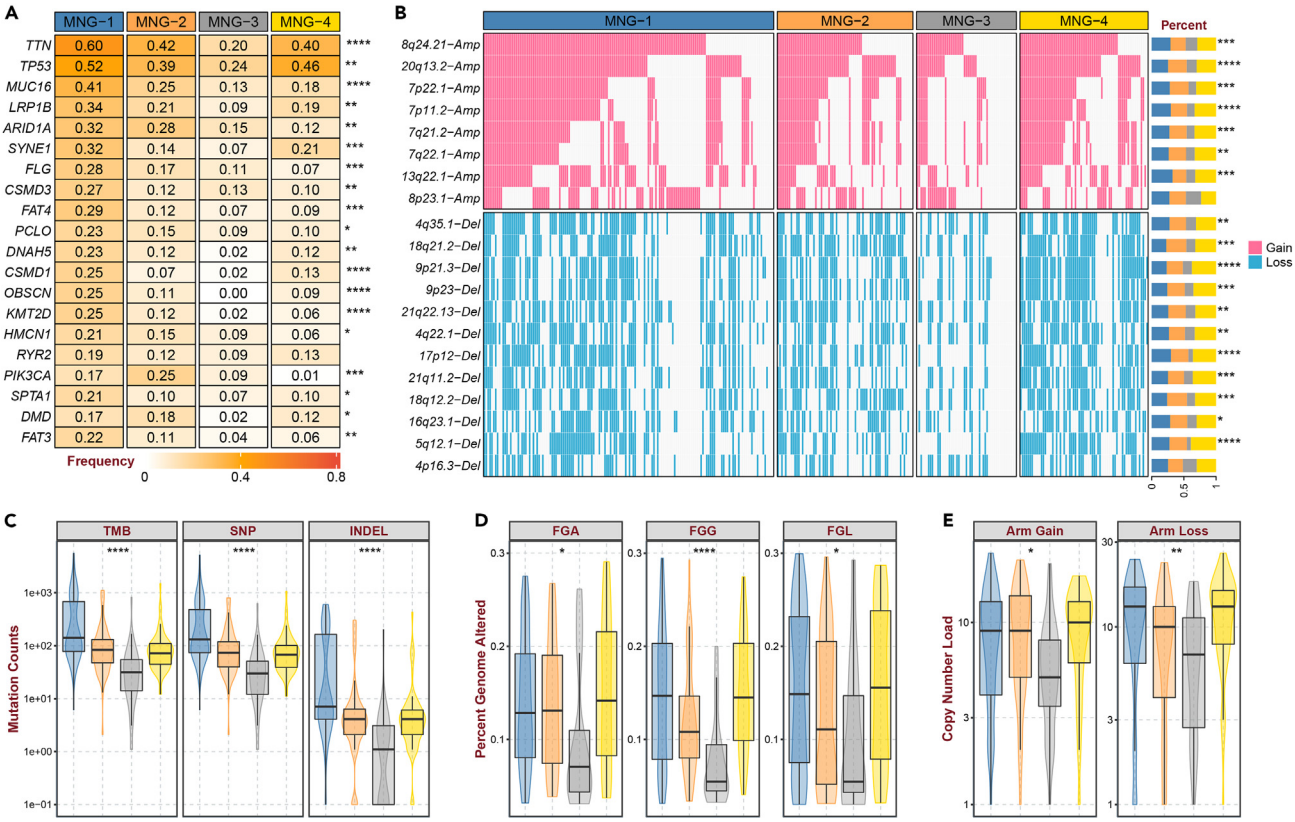

Figure 4. The genomic landscape of four subtypes

(A) Mutation frequency of the top 20 high-frequency gene mutations between four subtypes in the TCGA cohort.

(B) The heatmap includes the high-frequency chromosome copy number alterations in the GC samples.

(C) The amount of TMB, SNP, and INDEL between four subtypes.

(D) The CNV landscape between four subtypes at the focal level, including fraction genome altered (FGA), fraction genome gain (FGG), and fraction genome loss (FGL).

(E) The CNV landscape between four subtypes at the arm level. *p < 0.05, **p < 0.01, ***p < 0.001, and ****p < 0.0001. Data represent Q1 - 1.5*IQR to Q3 + 1.5*IQR (Q1: 25th percentile; Q3: 75th percentile; IQR: interquartile range).

(Figures 3A, S3C, and S3D). However, immune pathways also enriched in the MNG-3 subtype with lower normalized enrichment scores (Figures 3A and S3C).

For exploring the potential evolution of biological function among MNG-2, MNG-3, and MNG-4, the soft clustering method implemented in the *Mfuzz* package was conducted to identify ten gene clusters. Cluster 6 and 8 displayed the continuously changed expression pattern from MNG-2 to MNG-4 (Figure 3B). As expected, Cluster 6 was correlated with the extracellular matrix component, and Cluster 8 was related to immune response, which implied that the MNG-3 subtype perhaps keeps the functional status between MNG-2 and MNG-4 (Figures 3C and 3D). Comparing the two poor prognosis subtypes, MNG-4 displayed higher activities in the cell cycle, extracellular matrix disassembly, angiogenesis, and hypoxia pathways, while its immune-related pathway activities were significantly lower than those of MNG-3 (Figure S3E).

Significant genome variation was exhibited in MNG-1 and MNG-4

The overall level of genomic variation in four subtypes was indicated in the heatmap, including high-frequency mutated genes, copy number gain, and copy number loss (Figures 4A and 4B). We found significant differences in genomic variation among the four subtypes. As illustrated in detail, the MNG-1 subtype almost showed the highest mutation frequencies, especially TTN, TP53, MUC16, LRP1B, etc. In addition, MNG-4 also has a relatively higher mutation frequency of TP53, which is considered a key feature in CIN subtypes, and the lowest PIK3CA mutation (Figure 4A).[7] To compare the mutational load of the four subtypes more clearly, we calculated the tumor mutation burden (TMB), single-nucleotide polymorphism (SNP), and insertion and deletion (INDEL) for each patient. The results showed that MNG-1 still has the highest mutation level, followed by MNG-2 and MNG-4, while MNG-3 had the most barren mutation (Figure 4C). Subsequently, we further analyzed the copy number variant (CNV) levels of four subtypes, including the fraction of genome alteration, the fraction of genome gained, and the fraction of

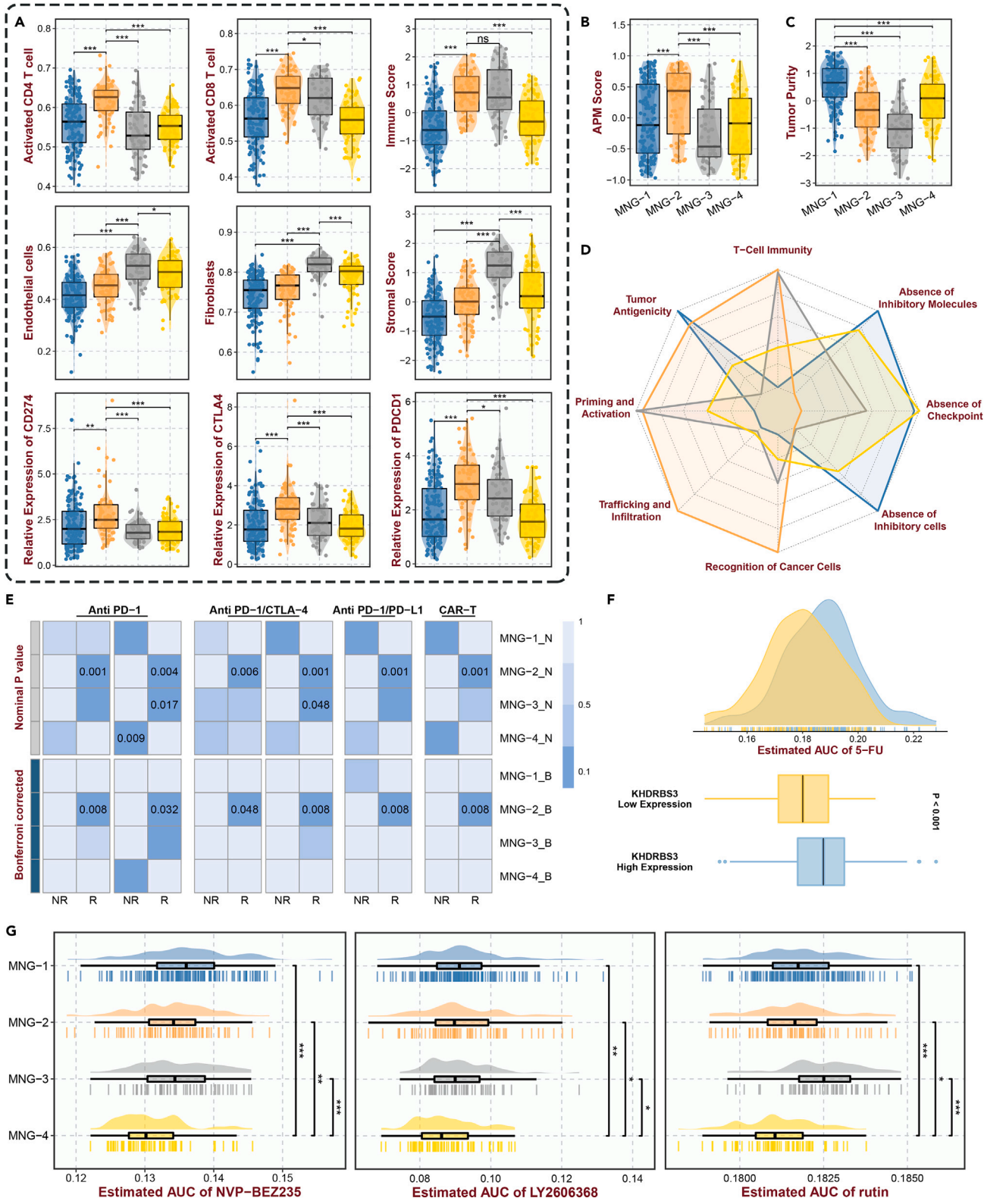
A
Activated CD4 T cell
Activated CD8 T cell
Immune Score
Endothelial cells
Fibroblasts
Stromal Score
Relative Expression of CD274
Relative Expression of CTLA4
Relative Expression of PDCD1
B
APM Score
MNG−1
MNG−2
MNG−3
MNG−4
C
Tumor Purity
D
T−Cell Immunity
Absence of Inhibitory Molecules
Absence of Checkpoint
Absence of Inhibitory cells
Recognition of Cancer Cells
Trafficking and Infiltration
Priming and Activation
Tumor Antigenicity
E
Anti PD−1
Anti PD−1/CTLA−4
Anti PD−1/PD−L1
CAR−T
Nominal P value
Bonferroni corrected
MNG−1_N
MNG−2_N
MNG−3_N
MNG−4_N
MNG−1_B
MNG−2_B
MNG−3_B
MNG−4_B
NR
R
F
Estimated AUC of 5−FU
KHDRBS3 Low Expression
KHDRBS3 High Expression
P < 0.001
G
MNG−1
MNG−2
MNG−3
MNG−4
Estimated AUC of NVP−BEZ235
Estimated AUC of LY2606368
Estimated AUC of rutin

Figure 5. The immune landscape and therapy exploration of MNG subtypes

(A) The infiltration abundance of activated $CD4^+$ T cell, activated $CD8^+$ T cell, endothelial cells, and fibroblasts was evaluated by the ssGSEA algorithm. The relative expression of CD274, CTLA4, and PDCD1 was evaluated in the TCGA cohort. The ESTIMATE algorithm evaluated the immune score and stromal score.

(B) The difference in APM score between four subtypes.

(C) The ESTIMATE algorithm in the TCGA cohort evaluated the tumor purity.

(D) Differences in the eight steps of the CIC immunogram in the four subtypes.

(E) SubMap algorithm evaluated the expression similarity and the immunotherapy responses between TCGA-STAD and GSE136961 (Anti-PD-1), GSE145996 (Anti-PD-1), GSE115821 (Anti-PD-1 & anti-CTLA-4), GSE126044 (Anti-PD-1 & anti-PD-L1), GSE91061 (Anti-PD-1 & anti-CTLA-4), and GSE100797 (CAR-T).

(F) Comparing AUC values of 5-FU between low and high KHDRBS3 expression group.

(G) Comparison of sensitivity to NVP-BEZ235, LY2606368, and rutin in four subtypes. ns means $p > 0.05$, *$p < 0.05$, **$p < 0.01$, and ***$p < 0.001$. See also Figure S4.

genome lost. Unlike MNG-2 and MNG-3, MNG-1 and MNG-4 performed higher CNVs, particularly in the MNG-4 subtype (Figure 4D). Noteworthily, the variation trends of the four subtypes in focal and arm positions were similar to CNVs (Figure 4E).

The microenvironment drives the heterogeneity among subtypes

Based on the results of GSEA and GSVA, we discovered that MNG-2 and MNG-3 were closely related to the immune pathways. The expression of 28 immune cells was further calculated via the single-sample GSEA (ssGSEA) algorithm to assess the abundance of immune infiltration in different subgroups. As shown in Figure S4A, the infiltration abundance was significantly more prominent in MNG-2, especially in activated $CD4^+$ T cell and activated $CD8^+$ T cell, verified by the immune score (Figure 5A). In contrast, the MNG-3 showed the highest stromal score and abundance of stromal cells, including endothelial cells and fibroblasts (Figure 5A). Subsequently, Figures S4B and S4C depict the differences in the expression of immune checkpoints (ICPs). The results revealed that the expression of ICPs was significantly higher in MNG-2, including the B7-CD28 superfamily, tumor necrosis factor (TNF) superfamily, and co-stimulatory ICPs, particularly CD274, CTLA4, and PDCD1 currently used in clinical practice, which suggested that the immune checkpoint inhibitors (ICIs) may be more effective in MNG-2 (Figure 5A). Additionally, MNG-2 also obtained higher scores in tumor inflammatory signature (Figure S4D) and antigen presentation score (Figure 5B), suggesting potentially better response and effect in immune activation and antigen presentation. Notably, MNG-2 and MNG-3 presented lower tumor purity and highly abundant infiltration of immune or stromal cells, which indicated that the tumor microenvironment may play a critical role in the two subtypes (Figure 5C). However, MNG-1 and MNG-4 appear barren regarding either infiltration of immune cells and immunomodulatory factors or immune scoring of the tumor microenvironment (Figure 5A). In particular, the MNG-4 subtype, in which various immune components regulating anti-tumor immunity showed low levels, may be an immune-desert microenvironment (Figure 5D).

Potential immunotherapy response for MNG-2

According to the immune landscape results, MNG-2 displayed higher immune cell infiltration and abundant ICPs, demonstrating that immunotherapy may be more applicable in this subtype. To further investigate the potential for immunotherapy response, we decoded the eight steps of the cancer immune cycle (CIC) immunogram to characterize anti-tumor immune processes. As illustrated in Figure 5D, CIC was a dynamic sequential process with seven steps, in which MNG-2 was prominent except for the absence of immune inhibition-related factors. Therefore, we performed the SubMap analysis between the discovery cohort and six independent cohorts with drug response information to identify the potential responder by similar expression profile pattern. As expected, the gene expression profiles of the MNG-2 subtype were significantly analogical with the immunotherapy responder meaning immunotherapy, such as anti-PD-1, anti-PD-L1, anti-CTLA4, and chimeric antigen receptor T-cell immunotherapy (CAR-T), is potentially beneficial to the MNG-2 patient (Figure 5E).

Potentially sensitive chemotherapy agents for MNG-4

Due to the undesirable prognosis in MNG-4 subtypes patients, we expected to find more effective drugs to improve the prognosis. Based on gene expression and drug sensitivity data from the Cancer Therapeutics Response Portal (CTRP) and profiling relative inhibition simultaneously in mixtures (PRISM) databases, we utilized area under the dose-response curve (AUC) values predicted by models to assess the drug sensitivity of GC patients. To validate the reliability of the method, we compared the AUC between low-KHDRBS3-expression and high-KHDRBS3-expression groups. The result showed that the low-KHDRBS3 group has a lower AUC value consistent with the previous study that low KHDRBS3 indicated high susceptibility for 5-fluorouracil (5-FU) (Figure 5F).[20] Then NVP-BEZ235, LY2606368, and rutin were recognized as better-sensitive drugs in MNG-4 patients by the differential comparison between the MNG-4 subtype and others (Figure 5G).

DISCUSSION

Due to the high tumor heterogeneity and invasiveness of GC, the AJCC staging system alone for clinical supervision and treatment decision-making no longer satisfies the demand for patient benefit.[21] With the development of immunology and molecular biology, PD-1/PD-L1-based ICPs have manifested resounding success in multiple solid tumors.[22] Although short-term survival has improved in partial GC patients with the management of immunotherapy-based combination therapy,[23] persistent reports of adverse immunotherapy reactions imply the disparate immunotherapy tolerance among GC patients.[24] Researchers have developed various GC molecular subtypes to change the status quo, but the clinical outcome is unsatisfactory. For the most part, the reason for this limited clinical transformation is that the transcriptional

classification based on gene expression is unstable and is highly susceptible to different sequencing platforms and temporal or spatial variation. Therefore, we constructed a GC molecular typing based on the immune gene interaction network, which capitally provides different insights for the refined management of GC patients.

In this study, we successfully classified GC patients into four subtypes based on immune gene networks. Notably, patients with the MNG-1 to MNG-4 subtype showed a progressive trend of deterioration. This unique prognostic value could help identify clinically high-risk patients and implement personalized interventions. However, favorable behavior in the TCGA cohort alone does not sufficiently account for the robustness of edge-perturbation typing. The reproducibility and stability of molecular subtypes are the prerequisites for clinical application.[25] Consequently, we further validated the edge-perturbation subtypes in 1,414 samples from four independent cohorts, showing a similar prognostic trend in all validation sets. It was worth emphasizing that the MNG-4 subtype similarly showed the most dismal prognosis in our collection of 90 GC samples. This multi-center, large-scale cohort validation lays a solid foundation for the future clinical application of edge-perturbation subtypes. In the comparative analysis of MNG subtypes with published GC subtypes, the CIN-like features of MNG-4 were not only manifested in the overlap of samples but also further confirmed by higher TP53 mutations and lowest PIK3CA mutations, as well as the highest frequency of copy number variations in genomic analysis. Accordingly, MNG-3 exhibits prevalent genetic hypomutation, consistent with the characteristics of the GS subtype. Although MNG-4 and MNG-3 have a relatively poorer prognosis and even a more pronounced trend for the former, the published subtypes associated with poor prognosis gather on MNG-3 and few on MNG-4, suggesting that MNG-4 may be a previously unrecognized subtype of poor prognosis.

As we know, significant prognostic differences in patients are generally caused by underlying biological mechanisms. Based on the functional enrichment analysis results, we discovered that the MNG-1 subtype is mainly associated with cell cycle pathways such as E2F targets, DNA replication, and mitotic sister chromatid segregation. However, activation of the G2M checkpoint pathway may be a favorable factor for good prognosis in the MNG-1 subtype. The MNG-2 subtype was primarily featured as an immune-hot subtype with a high abundance of immune-related pathways. We also recognized that the MNG-3 and MNG-4 subtypes exhibited powerful migratory and invasive features, especially epithelial-mesenchymal transition, a marker pathway of poor prognosis subtype in various tumors. Although MNG-3 and MNG-4 may be termed with EMT subtype, extracellular matrix remodeling characterized by angiogenesis and hypoxia, as well as the immune-desert microenvironment, in MNG-4 may provide potential interpretability for the metastatic propensity of this subtype.[26,27]

Immunotherapy, one of the foremost tumor treatments, has been granted a broad application prospect.[28] With the widespread clinical application of immunotherapy, how to accurately identify patients benefiting from immunotherapy has become an urgent problem to be solved. High immune cell infiltration and adequate activation of the anti-tumor immune program in MNG-2 further characterize its immune-hot subtype. Abundant immune cell infiltration, tumor antigen formation, and high expression of ICPs are the cornerstone of the response to ICPs (PD-1, PD-L1, CTLA-4, etc.) in tumor patients.[29] On top of that, we inferred that patients with the MNG-2 subtype have a higher immunotherapeutic benefit and validated it in six immunotherapy cohorts. Thus, edge-perturbation typing is confirmed as a vigoroso tool for immunotherapy decision-making in GC patients.

Despite the ability to accurately identify high-risk GC patients by edge-perturbation subtypes, establishing individualized treatment schemes for patients is the focus of clinical tasks. As an immune-desert state, patients with the MNG-4 subtype benefit minor from mainstream immunotherapy. Therefore, we used multiple drug sensitivity databases to compare drug sensitivity between subtypes. NVP-BEZ235, LY2606368, and rutin were the most sensitive in the MNG-4 subtype but less effective in the other three. Previous studies have shown that LY2606368, the checkpoint kinase 1 inhibitor, induced DNA damage, significantly inhibited cancer proliferation, and induced apoptosis in GC cells.[30] Rutin is a flavonoid that has the potential to reverse 5-FU resistance in human GC cells and its growth inhibitory effect on drug-resistant GC cells.[31] NVP-BEZ235 is the dual phosphoinositide 3-kinase (PI3K)/mammalian target of rapamycin (mTOR) inhibitor. Dual approaches are promising as targeting multiple downstream effectors may delay or prevent treatment resistance.[32] Although the NVP-BEZ235 was explored in GC cell lines, there is a limitation in that it responded to the specific cell lines.[33] This may result from the different gene expression profiles of distinct GC cell lines. Therefore, establishing edge-perturbation subtypes will also contribute to the precision treatment of clinical patients.

In summary, we identified four subtypes from the molecular heterogeneity of GC through a stable gene interaction network and validated subtypes in seven independent cohorts. Disparate subtypes differed in survival, prognosis, biological functions, genomic alterations, immune landscape, and potential therapeutic agents. RNA profile of GC samples from our internal cohort further demonstrated the clinical universality of edge-perturbation subtypes. In particular, MNG-4 was considered a previously undefined subtype with a dismal prognosis, characterized by EMT, chromosomal instability, and immune-desert microenvironment. This subtype tended to metastasize and was resistant to immunotherapy, so potential therapeutic agents for this subtype predicted for patients of this subtype may help improve the prognosis of GC.

Limitations of study

Although the multi-center and large-scale cohort validation proves that our established edge-perturbation subtype has powerful clinical applicability, there are still some shortcomings. First, immunotherapy cohorts for GC patients are relatively lacking. Secondly, the samples included in the analysis were retrospective data and lacked prospective studies.

STAR★METHODS

Detailed methods are provided in the online version of this paper and include the following:

- KEY RESOURCES TABLE
- RESOURCE AVAILABILITY
  - Lead contact
  - Materials availability
  - Data and code availability
- METHOD DETAILS
  - Sources and collection of study data
  - Establishment of edge-perturbation matrix
  - Identification of network-based molecular subtypes
  - Subtype validation in independent cohorts
  - Functional enrichment analysis
  - Genomic variation analysis
  - Immunophenotyping exploration among subtypes
  - Prediction of potential drugs for patients with poor prognosis
- QUANTIFICATION AND STATISTICAL ANALYSIS

SUPPLEMENTAL INFORMATION

Supplemental information can be found online at https://doi.org/10.1016/j.isci.2023.107871.

ACKNOWLEDGMENTS

This study was supported by the Major Science and Technology projects of Henan Province (Grant No. 221100310100).

AUTHOR CONTRIBUTIONS

Conceptualization, Z.Q.L. and X.W.H.; Methodology, C.G.G., X.Y.F., and H.X.; Investigation, H.X., X.Y.F., and S.Y.W.; Writing - Original Draft, X.Y.F. and C.G.G.; Writing - Review & Editing, L.B.Q., L.L., L.B.W., and S.Y.W.; Funding Acquisition, X.W.H.; Resources, K.X.C. and B.L.; Supervision, X.W.H., Z.Q.L., and K.X.C.

DECLARATION OF INTERESTS

The authors declare that they have no competing interests.

Received: July 7, 2023
Revised: August 11, 2023
Accepted: September 6, 2023
Published: September 9, 2023

REFERENCES

1. Torre, L.A., Bray, F., Siegel, R.L., Ferlay, J., Lortet-Tieulent, J., and Jemal, A. (2015). Global cancer statistics, 2012. CA A Cancer J. Clin. *65*, 87–108. https://doi.org/10.3322/caac.21262.
2. Ben-Aharon, I., van Laarhoven, H.W.M., Fontana, E., Obermannova, R., Nilsson, M., and Lordick, F. (2023). Early-Onset Cancer in the Gastrointestinal Tract Is on the Rise-Evidence and Implications. Cancer Discov. *13*, 538–551. https://doi.org/10.1158/2159-8290.CD-22-1038.
3. Nishiguchi, Y., Oue, N., Fujiwara-Tani, R., Sasaki, T., Ohmori, H., Kishi, S., Mori, S., Mori, T., Ikeda, N., Matsumoto, S., et al. (2019). Role of Metastasis-Related Genes in Cisplatin Chemoresistance in Gastric Cancer. Int. J. Mol. Sci. *21*, 254. https://doi.org/10.3390/ijms21010254.
4. Kumar, V., Ramnarayanan, K., Sundar, R., Padmanabhan, N., Srivastava, S., Koiwa, M., Yasuda, T., Koh, V., Huang, K.K., Tay, S.T., et al. (2022). Single-Cell Atlas of Lineage States, Tumor Microenvironment, and Subtype-Specific Expression Programs in Gastric Cancer. Cancer Discov. *12*, 670–691. https://doi.org/10.1158/2159-8290.CD-21-0683.
5. Smyth, E.C., Gambardella, V., Cervantes, A., and Fleitas, T. (2021). Checkpoint inhibitors for gastroesophageal cancers: dissecting heterogeneity to better understand their role in first-line and adjuvant therapy. Ann. Oncol. *32*, 590–599. https://doi.org/10.1016/j.annonc.2021.02.004.
6. Lei, Z., Tan, I.B., Das, K., Deng, N., Zouridis, H., Pattison, S., Chua, C., Feng, Z., Guan, Y.K., Ooi, C.H., et al. (2013). Identification of molecular subtypes of gastric cancer with different responses to PI3-kinase inhibitors and 5-fluorouracil. Gastroenterology *145*, 554–565. https://doi.org/10.1053/j.gastro.2013.05.010.
7. Cancer Genome Atlas Research Network (2014). Comprehensive molecular characterization of gastric adenocarcinoma. Nature *513*, 202–209. https://doi.org/10.1038/nature13480.
8. Cristescu, R., Lee, J., Nebozhyn, M., Kim, K.M., Ting, J.C., Wong, S.S., Liu, J., Yue, Y.G., Wang, J., Yu, K., et al. (2015). Molecular analysis of gastric cancer identifies subtypes associated with distinct clinical outcomes. Nat. Med. *21*, 449–456. https://doi.org/10.1038/nm.3850.
9. Oh, S.C., Sohn, B.H., Cheong, J.H., Kim, S.B., Lee, J.E., Park, K.C., Lee, S.H., Park, J.L., Park, Y.Y., Lee, H.S., et al. (2018). Clinical and genomic landscape of gastric cancer with a mesenchymal phenotype. Nat. Commun. *9*, 1777. https://doi.org/10.1038/s41467-018-04179-8.
10. Yeoh, K.G., and Tan, P. (2022). Mapping the genomic diaspora of gastric cancer. Nat. Rev.

Cancer *22*, 71–84. https://doi.org/10.1038/s41568-021-00412-7.
11. Chen, Y., Gu, Y., Hu, Z., and Sun, X. (2021). Sample-specific perturbation of gene interactions identifies breast cancer subtypes. Briefings Bioinf. *22*, bbaa268. https://doi.org/10.1093/bib/bbaa268.
12. Sahni, N., Yi, S., Taipale, M., Fuxman Bass, J.I., Coulombe-Huntington, J., Yang, F., Peng, J., Weile, J., Karras, G.I., Wang, Y., et al. (2015). Widespread macromolecular interaction perturbations in human genetic disorders. Cell *161*, 647–660. https://doi.org/10.1016/j.cell.2015.04.013.
13. Dai, H., Li, L., Zeng, T., and Chen, L. (2019). Cell-specific network constructed by single-cell RNA sequencing data. Nucleic Acids Res. *47*, e62. https://doi.org/10.1093/nar/gkz172.
14. Hou, S., Zhang, P., Yang, K., Wang, L., Ma, C., Li, Y., and Li, S. (2022). Decoding multilevel relationships with the human tissue-cell-molecule network. Briefings Bioinf. *23*, bbac170. https://doi.org/10.1093/bib/bbac170.
15. Zavros, Y., and Merchant, J.L. (2022). The immune microenvironment in gastric adenocarcinoma. Nat. Rev. Gastroenterol. Hepatol. *19*, 451–467. https://doi.org/10.1038/s41575-022-00591-0.
16. Guo, Y., Nie, Q., MacLean, A.L., Li, Y., Lei, J., and Li, S. (2017). Multiscale Modeling of Inflammation-Induced Tumorigenesis Reveals Competing Oncogenic and Oncoprotective Roles for Inflammation. Cancer Res. *77*, 6429–6441. https://doi.org/10.1158/0008-5472.Can-17-1662.
17. Zhang, P., Yang, M., Zhang, Y., Xiao, S., Lai, X., Tan, A., Du, S., and Li, S. (2019). Dissecting the Single-Cell Transcriptome Network Underlying Gastric Premalignant Lesions and Early Gastric Cancer. Cell Rep. *27*, 1934–1947.e5. https://doi.org/10.1016/j.celrep.2019.04.052.
18. Li, K., Zhang, A., Li, X., Zhang, H., and Zhao, L. (2021). Advances in clinical immunotherapy for gastric cancer. Biochim. Biophys. Acta Rev. Canc *1876*, 188615. https://doi.org/10.1016/j.bbcan.2021.188615.
19. Liu, Y., Sethi, N.S., Hinoue, T., Schneider, B.G., Cherniack, A.D., Sanchez-Vega, F., Seoane, J.A., Farshidfar, F., Bowlby, R., Islam, M., et al. (2018). Comparative Molecular Analysis of Gastrointestinal Adenocarcinomas. Cancer Cell *33*, 721–735.e8. https://doi.org/10.1016/j.ccell.2018.03.010.
20. Ukai, S., Honma, R., Sakamoto, N., Yamamoto, Y., Pham, Q.T., Harada, K., Takashima, T., Taniyama, D., Asai, R., Fukada, K., et al. (2020). Molecular biological analysis of 5-FU-resistant gastric cancer organoids; KHDRBS3 contributes to the attainment of features of cancer stem cell. Oncogene *39*, 7265–7278. https://doi.org/10.1038/s41388-020-01492-9.
21. Li, Y., Xu, C., Wang, B., Xu, F., Ma, F., Qu, Y., Jiang, D., Li, K., Feng, J., Tian, S., et al. (2022). Proteomic characterization of gastric cancer response to chemotherapy and targeted therapy reveals new therapeutic strategies. Nat. Commun. *13*, 5723. https://doi.org/10.1038/s41467-022-33282-0.
22. Safi, M., Ahmed, H., Al-Azab, M., Xia, Y.L., Shan, X., Al-Radhi, M., Al-Danakh, A., Shopit, A., and Liu, J. (2021). PD-1/PDL-1 Inhibitors and Cardiotoxicity; Molecular, Etiological and Management Outlines. J. Adv. Res. *29*, 45–54. https://doi.org/10.1016/j.jare.2020.09.006.
23. Entezam, M., Sanaei, M.J., Mirzaei, Y., Mer, A.H., Abdollahpour-Alitappeh, M., Azadegan-Dehkordi, F., and Bagheri, N. (2023). Current progress and challenges of immunotherapy in gastric cancer: A focus on CAR-T cells therapeutic approach. Life Sci. *318*, 121459. https://doi.org/10.1016/j.lfs.2023.121459.
24. Zhu, L., Kalimuthu, S., Gangadaran, P., Oh, J.M., Lee, H.W., Baek, S.H., Jeong, S.Y., Lee, S.W., Lee, J., and Ahn, B.C. (2017). Exosomes Derived From Natural Killer Cells Exert Therapeutic Effect in Melanoma. Theranostics *7*, 2732–2745. https://doi.org/10.7150/thno.18752.
25. Liu, Z., Weng, S., Dang, Q., Xu, H., Ren, Y., Guo, C., Xing, Z., Sun, Z., and Han, X. (2022). Gene interaction perturbation network deciphers a high-resolution taxonomy in colorectal cancer. Elife *11*, e81114. https://doi.org/10.7554/eLife.81114.
26. Nowosad, A., Marine, J.C., and Karras, P. (2023). Perivascular niches: critical hubs in cancer evolution. Trends Cancer. https://doi.org/10.1016/j.trecan.2023.06.010.
27. Sun, Z., Shao, B., Liu, Z., Dang, Q., Guo, Y., Chen, C., Guo, Y., Chen, Z., Liu, J., Hu, S., et al. (2021). LINC01296/miR-141-3p/ZEB1-ZEB2 axis promotes tumor metastasis via enhancing epithelial-mesenchymal transition process. J. Cancer *12*, 2723–2734. https://doi.org/10.7150/jca.55626.
28. Rizvi, N., Ademuyiwa, F.O., Cao, Z.A., Chen, H.X., Ferris, R.L., Goldberg, S.B., Hellmann, M.D., Mehra, R., Rhee, I., Park, J.C., et al. (2023). Society for Immunotherapy of Cancer (SITC) consensus definitions for resistance to combinations of immune checkpoint inhibitors with chemotherapy. J. Immunother. Cancer *11*, e005920. https://doi.org/10.1136/jitc-2022-005920.
29. Liu, L., Liu, Z., Gao, J., Liu, X., Weng, S., Guo, C., Hu, B., Wang, Z., Zhang, J., Shi, J., et al. (2022). CD8+ T cell trajectory subtypes decode tumor heterogeneity and provide treatment recommendations for hepatocellular carcinoma. Front. Immunol. *13*, 964190. https://doi.org/10.3389/fimmu.2022.964190.
30. Yin, Y., Shen, Q., Zhang, P., Tao, R., Chang, W., Li, R., Xie, G., Liu, W., Zhang, L., Kapoor, P., et al. (2017). Chk1 inhibition potentiates the therapeutic efficacy of PARP inhibitor BMN673 in gastric cancer. Am. J. Cancer Res. *7*, 473–483.
31. Xu, G.Y., and Tang, X.J. (2017). Troxerutin (TXN) potentiated 5-Fluorouracil (5-Fu) treatment of human gastric cancer through suppressing STAT3/NF-κB and Bcl-2 signaling pathways. Biomed. Pharmacother. *92*, 95–107. https://doi.org/10.1016/j.biopha.2017.04.059.
32. Gobin, B., Battaglia, S., Lanel, R., Chesneau, J., Amiaud, J., Rédini, F., Ory, B., and Heymann, D. (2014). NVP-BEZ235, a dual PI3K/mTOR inhibitor, inhibits osteosarcoma cell proliferation and tumor development in vivo with an improved survival rate. Cancer Lett. *344*, 291–298. https://doi.org/10.1016/j.canlet.2013.11.017.
33. Fuereder, T., Wanek, T., Pflegerl, P., Jaeger-Lansky, A., Hoeflmayer, D., Strommer, S., Kuntner, C., Wrba, F., Werzowa, J., Hejna, M., et al. (2011). Gastric cancer growth control by BEZ235 in vivo does not correlate with PI3K/mTOR target inhibition but with [18F]FLT uptake. Clin. Cancer Res. *17*, 5322–5332. https://doi.org/10.1158/1078-0432.Ccr-10-1659.
34. Song, F., Yang, D., Liu, B., Guo, Y., Zheng, H., Li, L., Wang, T., Yu, J., Zhao, Y., Niu, R., et al. (2014). Integrated microRNA network analyses identify a poor-prognosis subtype of gastric cancer characterized by the miR-200 family. Clin. Cancer Res. *20*, 878–889. https://doi.org/10.1158/1078-0432.Ccr-13-1844.
35. Şenbabaoğlu, Y., Michailidis, G., and Li, J.Z. (2014). Critical limitations of consensus clustering in class discovery. Sci. Rep. *4*, 6207. https://doi.org/10.1038/srep06207.
36. Hoshida, Y. (2010). Nearest template prediction: a single-sample-based flexible class prediction with confidence assessment. PLoS One *5*, e15543. https://doi.org/10.1371/journal.pone.0015543.
37. Hoshida, Y., Brunet, J.P., Tamayo, P., Golub, T.R., and Mesirov, J.P. (2007). Subclass mapping: identifying common subtypes in independent disease data sets. PLoS One *2*, e1195. https://doi.org/10.1371/journal.pone.0001195.
38. Hänzelmann, S., Castelo, R., and Guinney, J. (2013). GSVA: gene set variation analysis for microarray and RNA-seq data. BMC Bioinf. *14*, 7. https://doi.org/10.1186/1471-2105-14-7.
39. Subramanian, A., Tamayo, P., Mootha, V.K., Mukherjee, S., Ebert, B.L., Gillette, M.A., Paulovich, A., Pomeroy, S.L., Golub, T.R., Lander, E.S., and Mesirov, J.P. (2005). Gene set enrichment analysis: a knowledge-based approach for interpreting genome-wide expression profiles. Proc. Natl. Acad. Sci. USA *102*, 15545–15550. https://doi.org/10.1073/pnas.0506580102.
40. Kumar, L., and E Futschik, M. (2007). Mfuzz: a software package for soft clustering of microarray data. Bioinformation *2*, 5–7. https://doi.org/10.6026/97320630002005.
41. Zhou, Y., Zhou, B., Pache, L., Chang, M., Khodabakhshi, A.H., Tanaseichuk, O., Benner, C., and Chanda, S.K. (2019). Metascape provides a biologist-oriented resource for the analysis of systems-level datasets. Nat. Commun. *10*, 1523. https://doi.org/10.1038/s41467-019-09234-6.
42. Liu, Z., Guo, Y., Yang, X., Chen, C., Fan, D., Wu, X., Si, C., Xu, Y., Shao, B., Chen, Z., et al. (2021). Immune Landscape Refines the Classification of Colorectal Cancer With Heterogeneous Prognosis, Tumor Microenvironment and Distinct Sensitivity to Frontline Therapies. Front. Cell Dev. Biol. *9*, 784199. https://doi.org/10.3389/fcell.2021.784199.
43. Wang, L., Liu, Z., Zhu, R., Liang, R., Wang, W., Li, J., Zhang, Y., Guo, C., Han, X., and Sun, Y. (2022). Multi-omics landscape and clinical significance of a SMAD4-driven immune signature: Implications for risk stratification and frontline therapies in pancreatic cancer. Comput. Struct. Biotechnol. J. *20*, 1154–1167. https://doi.org/10.1016/j.csbj.2022.02.031.
44. Mermel, C.H., Schumacher, S.E., Hill, B., Meyerson, M.L., Beroukhim, R., and Getz, G. (2011). GISTIC2.0 facilitates sensitive and confident localization of the targets of focal somatic copy-number alteration in human cancers. Genome Biol. *12*, R41. https://doi.org/10.1186/gb-2011-12-4-r41.
45. Guo, C., Liu, Z., Yu, Y., Liu, S., Ma, K., Ge, X., Xing, Z., Lu, T., Weng, S., Wang, L., et al. (2022). Integrated Analysis of Multi-Omics Alteration, Immune Profile, and Pharmacological Landscape of Pyroptosis-Derived lncRNA Pairs in Gastric Cancer.

Front. Cell Dev. Biol. *10*, 816153. https://doi.org/10.3389/fcell.2022.816153.

46. Thorsson, V., Gibbs, D.L., Brown, S.D., Wolf, D., Bortone, D.S., Ou Yang, T.H., Porta-Pardo, E., Gao, G.F., Plaisier, C.L., Eddy, J.A., et al. (2018). The Immune Landscape of Cancer. Immunity *48*, 812–830.e14. https://doi.org/10.1016/j.immuni.2018.03.023.
47. Chen, D.S., and Mellman, I. (2013). Oncology meets immunology: the cancer-immunity cycle. Immunity *39*, 1–10. https://doi.org/10.1016/j.immuni.2013.07.012.
48. Karasaki, T., Nagayama, K., Kuwano, H., Nitadori, J.I., Sato, M., Anraku, M., Hosoi, A., Matsushita, H., Morishita, Y., Kashiwabara, K., et al. (2017). An Immunogram for the Cancer-Immunity Cycle: Towards Personalized Immunotherapy of Lung Cancer. J. Thorac. Oncol. *12*, 791–803. https://doi.org/10.1016/j.jtho.2017.01.005.
49. Ayers, M., Lunceford, J., Nebozhyn, M., Murphy, E., Loboda, A., Kaufman, D.R., Albright, A., Cheng, J.D., Kang, S.P., Shankaran, V., et al. (2017). IFN-γ-related mRNA profile predicts clinical response to PD-1 blockade. J. Clin. Invest. *127*, 2930–2940. https://doi.org/10.1172/jci91190.
50. Wang, S., He, Z., Wang, X., Li, H., and Liu, X.S. (2019). Antigen presentation and tumor immunogenicity in cancer immunotherapy response prediction. Elife *8*, e49020. https://doi.org/10.7554/eLife.49020.
51. Yang, C., Chen, J., Li, Y., Huang, X., Liu, Z., Wang, J., Jiang, H., Qin, W., Lv, Y., Wang, H., and Wang, C. (2021). Exploring subclass-specific therapeutic agents for hepatocellular carcinoma by informatics-guided drug screen. Briefings Bioinf. *22*, bbaa295. https://doi.org/10.1093/bib/bbaa295.

STAR★METHODS

KEY RESOURCES TABLE

REAGENT or RESOURCE	SOURCE	IDENTIFIER
Deposited data		
Relevant transcriptomic data, clinical data, and somatic mutation data of TCGA-STAD cohort	The TCGA data portal	https://portal.gdc.cancer.gov/
Transcriptomic data of normal gastric tissues	The UCSC Xena database	https://xenabrowser.net/datapages/
Transcriptomic data	Gene Expression Omnibus database	GSE15459
Transcriptomic data	Gene Expression Omnibus database	GSE26253
Transcriptomic data	Gene Expression Omnibus database	GSE84433
Transcriptomic data	Gene Expression Omnibus database	GSE84437
Gene expression data of cell lines	The Cancer Cell Line Encyclopedia database	https://sites.broadinstitute.org/ccle/
Drug sensitivity data	The cancer therapeutics response portal	https://portals.broadinstitute.org/ctrp.v2.1/
Drug sensitivity data	The PRISM lab	https://www.theprismlab.org/
Immune genes	The ImmPort Portal	https://www.immport.org
Software and algorithms		
R (version 4.1.2)	the R Core Team and the R Foundation for Statistical Computing	https://www.r-project.org/
ConsensusClusterPlus	R Bioconductor	RRID:SCR_016954
limma	R Bioconductor	RRID:SCR_010943
CMScaller	GitHub	https://github.com/peterawe/CMScaller
clusterProfiler	R Bioconductor	RRID:SCR_016884
maftools	R Bioconductor	N/A
pRRophetic	GitHub	https://github.com/paulgeeleher/pRRophetic
Other		
In-house cohort	Song et al.	https://doi.org/10.1158/1078-0432.CCR-13-1844

RESOURCE AVAILABILITY

Lead contact

Further information and request for resources should be directed and will be fulfilled by the lead contact, Xinwei Han (fcchanxw@zzu.edu.cn).

Materials availability

This study did not generate new unique reagents.

Data and code availability

- Public data used in this work can be acquired from the TCGA (https://portal.gdc.cancer.gov/), GEO (https://www.ncbi.nlm.nih.gov/geo/), and the UCSC-Xena (https://xenabrowser.net/datapages/) database.
- The code used in this study mainly relies on existing R packages, which are described in the STAR methods.
- Any additional information required to reanalyze the data reported in this paper is available from the lead contact upon request.

METHOD DETAILS

Sources and collection of study data

A total of 1762 GC samples from five independent cohorts were collected in the study, including TCGA-STAD (n = 348), GSE15459 (n = 192), GSE26253 (n = 432), GSE84433 (n = 357), GSE84437 (n = 433), from the Cancer Genome Atlas (TCGA, https://portal.gdc.cancer.gov/) portal and Gene Expression Omnibus database (GEO, https://www.ncbi.nlm.nih.gov/geo/). Transcriptome data obtained by microarray analysis of 90 GC samples from Tianjin Medical University Cancer Institute and Hospital were included. Details of baseline information about six public datasets and an in-house cohort were summarized in Table S1. In addition, expression profiles of 174 normal gastric tissues were retrieved

from the UCSC-Xena database (https://xenabrowser.net/datapages/). RNA-sequencing data were processed to transcripts per million (TPM) format and normalized by log2 transformation. Somatic mutation and copy number variation data were also downloaded from the TCGA database. For further exploration of immunotherapy responses, six cohorts from GEO with complete immunotherapy information were recruited, including GSE100797 (CAR-T), GSE115821 (Anti-PD-1 & anti-CTLA-4), GSE126044 (Anti-PD-1 & anti-PD-L1), GSE136961 (Anti-PD-1), GSE145996 (Anti-PD-1), and GSE91061 (Anti-PD-1 & anti-CTLA-4). Gene expression data of cell lines were obtained from the Cancer Cell Line Encyclopedia (CCLE, https://sites.broadinstitute.org/ccle/), and drug sensitivity data were downloaded from the cancer therapeutics response portal (CTRP, https://portals.broadinstitute.org/ctrp.v2.1/) and the profiling relative inhibition simultaneously in mixtures (PRISM, https://www.theprismlab.org/).

Processing of transcriptome data in the Tianjin cohort.

In this study, the Tianjin cohort (n = 90) was included as an internal validation cohort, which comprised 90 GC patient samples from Tianjin Medical University Cancer Hospital.[34] GC samples were processed as follows: (1) TRIzol Reagent (Invitrogen) and ethanol precipitation were used to extract and purify the RNA. (2) Nano-Drop-8000 was used to detect the concentration and quality of RNA. (3) After analysis and processing of Affymetrix GeneChip HT HG-U133+PM 96-array plates, the microarray was scanned by The GeneTitan Instrument (Affymetrix) to obtain expression profile data. The Institutional Review Board of Tianjin Medical University approved the study, and all patients provided informed consent.

Establishment of edge-perturbation matrix

To identify molecular subtypes of GC with gene interaction information, we developed an edge-perturbation matrix based on immune genes in a cohort of gastric cancer patients. The construction process of this matrix is detailed below.

1) **Obtain edges of immune gene interaction.** A total of 1793 immune genes were identified from the ImmPort Portal (https://www.immport.org). Subsequently, all immune genes were input into the STRING database. For screening genes with biological interactions, the connection strength was set to 0.7, and 15,347 edges of gene interaction were obtained as the background network.
2) **Construct the edges of gene interactions.** Genes were ranked based on the average expression level in all normal samples from GTEx. Notably, the rank difference between genes was used to reflect their degree of interaction. The edges of gene interactions were calculated according to the formula:

$$E_{Gi\text{-}Gj} = R_{Gi}\text{-}R_{Gj}$$

Gi represented the ith gene, R_{Gi} represented the rank of Gi, and $E_{Gi\text{-}Gj}$ represented the edge-perturbation value of Gene i and Gene j. Additionally, rank differences after ordering the average expression of genes based on 174 normal samples were calculated to generate edge benchmarks.
3) **Generate the GC edge-perturbation matrix.** The edges of gene interactions in each tumor sample subtracting the benchmark generated the edge-perturbation matrix for further analysis.

Identification of network-based molecular subtypes

The *ConsensusClusterPlus* package was used to identify molecular subtypes based on the edge-perturbation matrix. The ConsensusClusterPlus function was configured with the following criteria: the maximum number of clusters set to 10, 100 iterations, pItem set to 0.8, and utilizing the Partitioning Around Medoid (PAM) clustering algorithm with Euclidean distance. The number of candidate clusters k ranged from two to ten, and the optimal k value was determined based on the cumulative distribution function (CDF).[35]

Subtype validation in independent cohorts

Differential expression analysis between subtypes was performed using the *limma* package in the discovery cohort to determine the characteristic genes for individual subtypes. Furthermore, subtype-specific genes were identified using Tukey's range multiple testing with Holm's correction. Based on the feature genes of each subtype, we predicted the typing of samples via the nearest template prediction (NTP) algorithm of the *CMScaller* package.[36] The samples with FDR <0.2 are considered to assign an MNG subtype successfully. The concordance of transcriptional profiles for each subtype across cohorts was verified by the Subclass Mapping (SubMap) algorithm,[37] and Bonferroni corrected $p < 0.05$ was considered statistically significant.

Functional enrichment analysis

To ascertain the specific biological functions of the four GC subtypes, gene set variation analysis (GSVA) was adopted.[38,39] The gene sets were downloaded from the molecular signatures database (MsigDB), including c5.go.v7.5.1.symbols.gmt, c2.cp.kegg.v7.5.1.symbols.gmt, and h.all.v7.5.1.symbols.gmt. Gene set enrichment analysis (GSEA) was implemented by the *clusterProfiler* package. The differential analysis in four subtypes was executed, and the genes were ranked in descending order according to log2FoldChange (log2FC). Normalized enrichment score (NES) represented the enrichment score of gene sets in subtypes, and $p < 0.05$ was considered statistically significant. Subsequently, GSVA converted the gene expression matrix into the variance score matrix, and subtype-characterized pathways were identified by analysis of differences between groups with adjusted $p < 0.05$. In addition, Metascape was used to functionally characterize the signature gene clusters resulting from the soft clustering method (Mfuzz).[25,40,41]

Genomic variation analysis

Somatic mutations and copy number variants (CNVs) characteristics were utilized to compare differences in the genomics of the four subtypes.[42,43] Firstly, we calculated gene mutation frequencies via the *maftools* package, and the top 20 were singled out as high-frequency mutated genes. To further compare the difference in mutation burden among different subtypes, the tumor mutation burden (TMB) was calculated, which includes single nucleotide polymorphisms (SNP) and insertion and deletion (INDEL). The CNVs of each patient in the TCGA cohort were deciphered via the GISTIC 2.0 algorithm. Additionally, the box diagram further depicted the CNVs of different subtypes in focal- and arm-levels.[44]

Immunophenotyping exploration among subtypes

To assess the immune infiltration microenvironment, we decoded the infiltration abundance of 28 immune cells in GC patients by the single sample gene set enrichment analysis (ssGSEA) algorithm.[45] Subsequently, the expression of immune molecules among different subtypes was compared in more detail, including the B7-CD28 superfamily, TNF superfamily, immune co-stimulatory, and immune co-inhibitory checkpoints.[46] The cancer immune cycle (CIC),[47] also known as the anti-tumor immunity process, consists of seven steps, including cancer cell antigens, cancer antigen presentation, priming and activation of effector T cells, T cell migration to cancer tissue, infiltration of immune cells into tumors, recognition of cancer cells by the T cell, and killing of cancer cells. As a previous study reported,[48] different GC subtypes were impaired at eight stages of CIC immunogram and exhibited distinct endogenous immune escape mechanisms. Notably, to better assess the ability of patients to respond to immunotherapy, three approaches were undertaken: (1) Tumor inflammatory signature (TIS) score, composed of 18 immune-inflammatory genes, was conducive to predicting clinical response to PD-1 blockade.[49] (2) The antigen processing and presenting machinery scores (APS) were calculated based on 16 antigen-presenting genes, which unfold the efficiency of antigen processing and delivery.[50] (3) In six immunotherapy cohorts, the Submap was adopted to compare the expression profiles between immunotherapy responders and each subtype for predicting the potential responder of immunotherapy, such as anti-PD-1 and anti-CTLA-4.

Prediction of potential drugs for patients with poor prognosis

We obtained massive gene expression and drug-sensitive information from the CTRP and PRISM databases. As previously reported,[51] the ridge regression model implemented in the *pRRophetic* package was used for predicting drug response, and the prediction accuracy was performed by 10-fold cross-validation. The drug with the smaller AUC was considered more sensitive for the GC patient. The potential susceptibility drugs for the subtype with the poorest prognosis were determined by the differential comparison in AUC values.

QUANTIFICATION AND STATISTICAL ANALYSIS

All data analysis and visualization were performed in R software (version 4.1.2). Kaplan-Meier survival and Cox regression analysis were conducted by the *survival* package. Comparisons of categorical variables were performed by the chi-square test or Fisher exact test, and comparisons of continuous variables were performed by the Wilcoxon rank-sum test or the t-test. $p < 0.05$ was considered statistically significant, and all statistical tests were on two sides.